This is the accepted manuscript made available via CHORUS. The article has been published as:

# Cooling rate and stress relaxation in silica melts and glasses via microsecond molecular dynamics

J. Matthew D. Lane

# Cooling rate and stress relaxation in silica melts and glasses via microsecond molecular dynamics

J. Matthew D. Lane

*Sandia National Laboratories, Albuquerque, NM 87185*

We have conducted extremely long molecular dynamics (MD) simulations of glasses to microsecond times, which close the gap between experimental and atomistic simulation timescales by 2 to 3 order of magnitude. Static, thermal, and structural properties of silica glass are reported for glass cooling rates down to $5 \times 10^9$ K/s and viscoelastic response in silica melts and glasses are studied over 9 decades of time. We present results from relaxation of hydrostatic compressive stress in silica and show that time-temperature superposition holds in these systems for temperatures from 3500 K to 1000 K.

## I. INTRODUCTION

Silica is a ready glass former which is commonly studied experimentally, theoretically and computationally, as a model material for strong glass formation. Atomistic simulation of silica has provided a molecular window into the structure and the dynamics that dictate the various regimes of glassy response.

Silica is known to locally form well-defined tetrahedra of $SiO_4$, where silicon forms the tetrahedral center with oxygen surrounding. Each oxygen, in turn, bridges the tetrahedral corners, bonding between two silicon centers. The glassy disorder at mid- and long-range comes from the variation in orientation of adjacent tetrahedra. Silica structure has been studied experimentally using neutron diffraction as well as by simulation. In some cases, the timescales of molecular simulation overlap well with those of the dominant physics, as in the study of mode-coupling theory (MCT) where nanosecond times are sufficient to validate the theory in supercooled silica above 3300 K. However, at lower temperatures, the physical timescales quickly extend by orders of magnitude.

Molecular dynamics (MD) has been extensively used to study silicate glasses [1–3] in areas of nanosecond aging of silica [4–6], pressure and shear response [7–9], and cooling-rate effects [10–13]. In this work, we use the BKS interatomic potential [14], which has been used frequently to study the glass properties of silica, and has been demonstrated to capture experimentally observed behavior. Horbach and Kob [15] showed that BKS predictions agreed well with experimental $SiO_2$ neutron scattering experiments [16]. They also showed that BKS dynamic results agreed well with mode-coupling theory above a calculated critical temperature $T_c$ of 3330 K. This value agreed with extrapolations from prior experimental data [17]. Vollmayr, *et al.* [18] showed that the potential captures silica's anomalous density dependence on temperature. The BKS potential captures the qualitative features of the density maximum, but overpredicts the temperature of the peak at 4800 K compared to experimental observations [19, 20] near 1800 K. Direct comparison of the glass transition temperature, $T_g$ is not possible because $T_g$ is a function of the cooling rate, and cooling rates differ greatly between experiment and simulation. Two papers have attempted to extrapolate simulation $T_g$ out to experimental rates. Vollmayr, *et al.* [18] calculated 2525 K, while Horbach and Kob [15] calculated 1380 K, compared to the experimental value of $T_g = 1446$ K[21]. In both cases, the extrapolations were made across cooling rates that differed by 8 to 10 orders of magnitude.

The BKS potential has also been used to explore the fragile-to-strong transition in silica [15, 22, 23]. The fragile-to-strong transition refers to the change in viscosity dependence on temperature from super-Arrhenius to Arrhenius behavior in the temperature range of 3300 K to 4000 K. Our simulations of stress relaxation explore a range of temperatures which almost exclusively sample melts/glasses below this transition, where silica is a strong glass.

In this work, we extend the accessible timescales of molecular simulation of silica to microseconds. We begin with a brief summary of our simulation approach and methodology, followed by our results, reported in two subsections. First, we present the effect of extended cooling rates on the macroscopic and microscopic properties of glass structure. Second, we report the long-time stress relaxation properties of silica glass, including explicit testing of the viscoelastic property of time-temperature superposition and the mechanisms for stress relaxation via subtle structural relaxation.

## II. METHODOLOGY

Classical MD simulation was used to model the microsecond behavior of silica glass, using Sandia's LAMMPS [24] code. Silica was modeled with the BKS interatomic potential [14], with long-range electrostatics, as shown in Equation 1. The BKS potential has been shown to capture much of the behavior of silica glass with a highly efficient two-body interaction. The potential combines a Coulomb interaction with an exponential core repulsion and a dispersion term. The exponential and dispersion terms were cutoff at 1.0 nm. The long-range electrostatics were calculated with the PPPM algorithm [25] with accuracy of $10^{-4}$. A time step of 1.0 fs was used, throughout. The BKS interatomic potential, as

| | $A_{ij}$ (Kcal/mol) | $b_{ij}$ (1/Å) | $c_{ij}$ (Kcal/mol Å$^6$) | $F_{ij}^0$ (eV/Å) | $V_{ij}^0$ (Kcal/mol) | $K$ (Kcal/mol/Å$^2$) | Charge |
|---|---|---|---|---|---|---|---|
| **Si-O** | 415 182.844 | 4.87318 | 3 079.50877 | 1 187.85 | 376.5 | 1000.0 | $q_{Si} = 2.4$ |
| **O-O** | 32 026.355 | 2.76000 | 4 035.6575 | 1 441.37 | 1372 | 1000.0 | $q_O = -1.2$ |

TABLE I: Interatomic potential parameters for BKS silica with modified harmonic core.

with all Buckingham-style potentials, is known to have an unphysical and undesired run-away attractive core when atoms get closer than a critical radius. Although rare, this can cause problems in high-temperature melts. We follow Vollmayr *et al.* [18] in correcting this deficiency by replacing the potential with a harmonic core (Equation 2) for $r_{ij} < R_c$, where $R_c^{Si-O} = 1.188$ Å and $R_c^{O-O} = 1.441$ Å.

$$V_{ij} = \frac{q_i q_j}{r_{ij}} + A_{ij} e^{-b_{ij} r_{ij}} - \frac{c_{ij}}{r_{ij}^6} \qquad r_{ij} \geq R_c \qquad (1)$$

$$V_{ij} = \frac{1}{2} K r_{ij}^2 - F_{ij}^0 r_{ij} + V_{ij}^0 \qquad r_{ij} < R_c \qquad (2)$$

where the values for the parameters $q_i$, $A_{ij}$, $b_{ij}$, $c_{ij}$ (unchanged from Ref. [14]), $F_{ij}^0$ and $V_{ij}^0$ and $K$ are given in Table I. $F_{ij}^0$ and $V_{ij}^0$ were calculated so that energy and force are continuous at $R_c$. The potential is implemented through a LAMMPS pair_table, which is available from the author upon request.

The glass systems were created from $\beta$-cristobalite crystal through a melt-quench process. The initial crystal was melted with a linear temperature ramp from 300 K to 8000 K over 0.1 ns. The melt was then equilibrated for 2.2 ns at 8000 K to remove all residual order from the original crystal, before a linear temperature quench was imposed to 300 K to rapidly resolidify the silica. The cooling rate was varied from $7.7 \times 10^{13}$ K/s to $5 \times 10^9$ K/s to study the effect of the quench rate on the properties of the glass. These rates correspond to simulation times of 0.1 ns and 1 $\mu$s, respectively. Silica samples of relatively modest size were used so that the systems could be run efficiently for very long times. Samples consisted of 13,824 atoms with dimensions of 12.0 nm × 4.5 nm × 2.5 nm with periodic boundary conditions in all directions. During the equilibration and temperature ramps a constrained pressure and temperature (NPT) ensemble was used, with the pressure held at 1 atm. A Nosé-Hoover damping coefficient of 100 fs was used to couple the thermostat and 1000 fs was used to couple the barostat.

For the stress relaxation simulations, compression was imposed by a hydrostatic affine deformation strain applied to produce a 3% volumetric strain. This strain was imposed instantaneously, which produced an immediate stress on the system. The systems were then held in a constrained volume and energy (NVE) ensemble with an additional weak Langevin thermostat to prevent energy drift over very long simulation times. The thermostat damping coefficient was 1 ps. The initial glass had been cooled at $5 \times 10^{11}$ K/s for these simulations, and had a density of 2.24 g/cc. The longest simulations were run out to a billion timesteps, which each took more than six months of wall time on 8 cores.

Due to the very long simulations runs, we opted to study larger systems, using spatial averaging rather than averaging over multiple simulation instances as is often done. We found that the larger system averages were quite smooth, and gave good statistics. Comparison with previously published results [18], which averaged 20 instances of much smaller (1002 atoms vs our 13,824 atoms) simulations, showed very good agreement, even when the systems had clearly diverged from equilibrium.

### III. RESULTS

#### A. Glass property dependence on cooling rate

Cooling rates in experimentally cooled glasses are often on the timescale of degrees per second or degrees per minute, whereas atomistic simulations cool glasses at trillions of degrees per second. This mismatch of timescale is sometimes bridged with theory, and sometimes ignored. It has been shown for instance that glass/melt diffusion rates and glass transition rates can be scaled across this
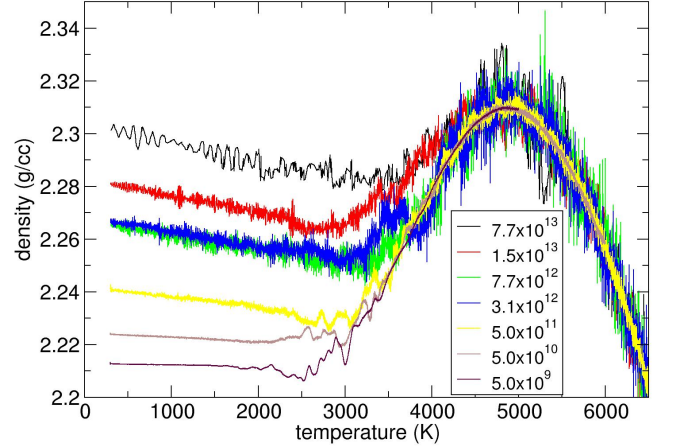


FIG. 1: (Color online) Plot of the density vs temperature for seven glass quenches completed with linear cooling rates, $\gamma$, ranging from $7.7 \times 10^{13}$ down to $5 \times 10^9$. All quenches qualitatively capture silica's anomalous density. Density, $\rho(T)$, is independent of ramp rate down to approximately 4500 K.
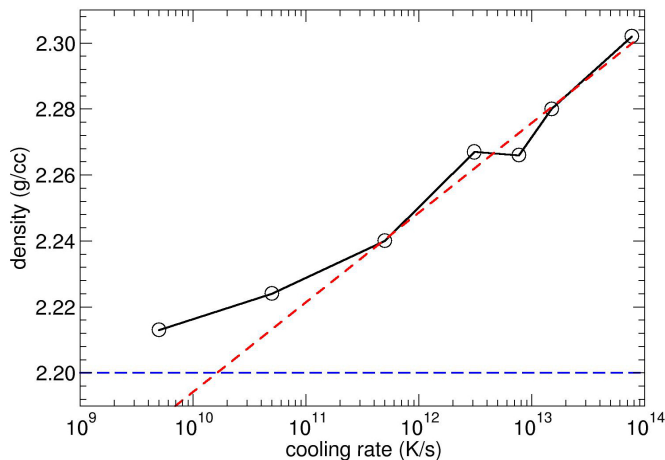
FIG. 2: (Color online) Plot of density, $\rho$, at 300 K, as a function of the glass quench cooling rate, $\gamma$. The blue dashed line is the experimental value. The red dashed line is a linear extrapolation fit to data in the range above $3 \times 10^{12}$. The statistical error is smaller than the data points.

huge data gap [15]. Another approach is simply to measure macroscopic glass properties and structure and show that they are in reasonable agreement, regardless of the glass-formation procedure. [1]

Here, we extend the glass cooling rate in atomistic simulation by 2 to 3 order of magnitude over previous studies, down to $5 \times 10^9$ K/s. Vollmayr, *et al.* [18] presented a similar study, but computational considerations limited their slowest cooling rate to $3 \times 10^{12}$ K/s. We reproduce to good accuracy previously reported data where it overlaps our current cooling rates, as noted below.

Figure 1 shows a plot of the density dependence of silica for quench rates ranging from $7.7 \times 10^{13}$ K/s to $5.0 \times 10^9$ K/s. The figure should be read from right to left, as temperatures are linearly ramped downward. The silica density anomaly is clearly seen as the hump in the data near 4800 K. Above this peak, the density-temperature relationship is independent of quench rate. To the left of the peak, below 4500 K, as temperatures continue to drop the system turns glassy and the density is strongly dependent on the rate of quench. Densities at low temperature differ by approximately 5% over the range of quench rates explored here. Below 2000 K, the density response for all rates shows a typical solid-like linear thermal contraction with decreasing temperature. The onset of this regime is rate dependent, ranging from 2000 to 3000 K. Data was recorded every 0.1 ps during the quench and density is averaged in 1 kelvin bins. Thus, the slower ramp rates appear smoother due to improved statistical averages, but all rates show comparable density fluctuations for a given temperature.

Figure 2 shows the final density of each glass at 300 K plotted as a function of cooling rate, $\gamma$, on a semi-log plot. These data are the final densities from the quench curves shown in Fig. 1. Error bars are smaller than the

data points. The results capture silica's unusual characteristic of density decrease for decreasing cooling rate. In most glasses, density increases as cooling rates are slowed. The unusual trend in silica is due to the density hump anomaly, discussed above. The slowest cooling rates show a divergence from linear, perhaps, toward an asymptotic approach to the experimental value of 2.20 g/cc (blue dashed). However, we note that predicting the onset of asymptotic behavior is difficult. Vollmayr et al [18], argued that such an asymptote was not possible since for very small cooling rates the density would need to invert and begin to increase with decreasing cooling rate. We see no evidence of such an inversion at the rates we modeled. The red dashed line is a linear fit to our data above $3 \times 10^{12}$ K/s cooling rates and extrapolated to $10^{10}$ K/s. Comparing this extrapolated trend from the higher rates with our measured data below $10^{12}$ K/s highlights the nonlinear (possibly asymptotic) response.

The thermal expansion coefficients of the final glasses also depend on the rate at which it was cooled. The thermal expansion coefficient at constant pressure, $\alpha_P$ can be calculated from discrete simulation by

$$\alpha_P = \frac{1}{\rho}\frac{\Delta\rho}{\Delta T} \tag{3}$$

where $\rho$ is the density and $T$ is the temperature. Graphically, the thermal expansion corresponds to the slope in density vs temperature curves such as in Figure 1. The error bars, here also, are smaller than the data point. Figure 3 shows $\alpha_P$ as a function of the cooling rate, on a semi-log plot, evaluated between 300 and 800 K.. The data can be reasonably fit with a linear trend in $\alpha_P$ vs $\log(\gamma)$. However, the trend appears to soften at both the high and low ends of this range of cooling rates. The
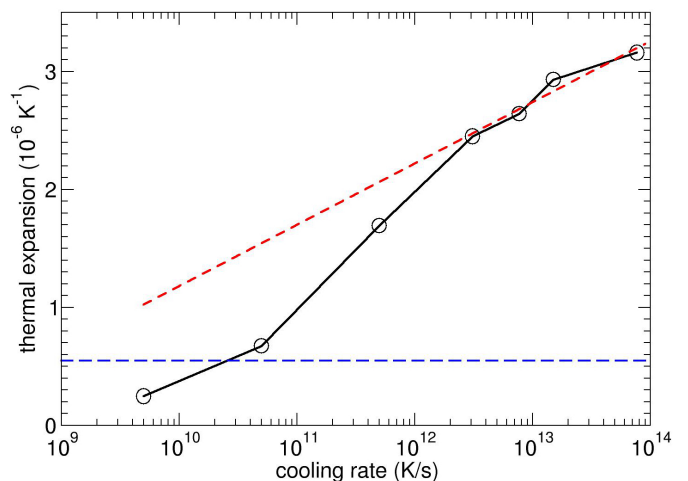


FIG. 3: (Color online) Plot of the thermal expansion coefficient at constant pressure, $\alpha_P$, calculated at 300 K, as a function of the glass quench cooling rate, $\gamma$. The blue dashed line is the experimental value. The red dashed line is a linear extrapolation fit to data in the range above $3 \times 10^{12}$. The statistical error is smaller than the data points.
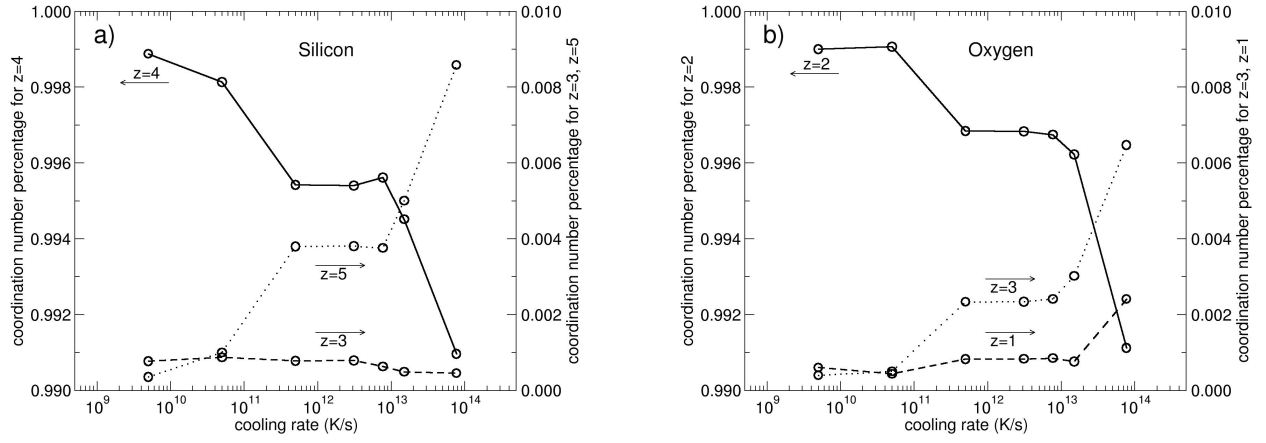
FIG. 4: Partial coordination number $z$ as a function of glass cooling rate, $\gamma$. (a) Silicon coordination number with oxygen, (b) Oxygen coordination number with silicon. Optimal coordination is z=4 for silicon, and z=2 for oxygen.

experimental value of the thermal expansion coefficient [26] is also shown with a blue dashed line. Here, it is not possible to argue that the high-rate simulation results asymptotically approach the low-rate experimental value, as the value for $5 \times 10^9$ K/s crosses below the experimental value. As in Figure 2, the red dashed line in Fig. 3 is a linear fit to our data above $3 \times 10^{12}$ K/s and extrapolated to $10^{10}$ K/s. We measured thermal expansion coefficients significantly below what would have been expected by extrapolating from higher cooling rates.

We turn now to the microscopic dependence of glass structure on cooling rate, with investigation of the partial coordination numbers, bond angle distributions and the radial distribution functions for glasses of different cooling rates.

A primary measure of microscopic structure is the coordination number of atoms within a glass. The coordination number $z$ gives the number of neighbors within a given radius of an atom. In silica, the silicon-centered tetrahedra give dominant coordination numbers of $z = 4$ for silicon and $z = 2$ for oxygen, for $r_{\text{Si}-\text{O}} = 0.215$ nm. But, over- and under-coordination are always present in glassy states, and give us information about the relaxation of the glass structure.

Figure 4 shows the probability of finding various coordinations numbers in Si and O for glasses formed at various cooling rates. We observe that as rates of cooling decrease, we see a higher percentage of perfect tetrahedral coordination number for both silicon and oxygen. Even at our highest cooling rate of $7.7 \times 10^{13}$ K/s fewer than 10 in 1000 silicon atoms have other than $z = 4$, and a similar percentage of oxygen atoms have other than $z = 2$. Vollmayr, et al. have previously reported that the over- and under-coordination rates drop rapidly with cooling rate down to approximately $1 \times 10^{13}$ K/s and then appear to plateau below that. Our results agree with this down to rates of $5 \times 10^{11}$ K/s, but we show that at still slower cooling rates, the over-coordination drops further. This is particularly interesting since for

both silicon and oxygen, the continued drop brings the over-coordination and under-coordination of both silicon and oxygen into parity. At the higher cooling rates, over-coordination is always dominant. At our slowest cooling rate of $5 \times 10^9$ K/s only approximately one silicon atom out of every thousand has other than perfect tetrahedral coordination. This reduction in non-ideal structure, and particularly the reduction of over-coordination appears consistent with trends in density with decreasing cooling rate.

A common quantitative measure of the bonding structure is the radial distribution function (rdf) [27], which measures the average order between atom pairs in a material and is given by

$$\text{rdf}(r_n) = \frac{V h_n}{2\pi N^2 r_n^2 \Delta r} \tag{4}$$

where $V$ is the total volume, $N$ is the total particle number, $h_n$ is the count within the $n$th radial shell whose center is a distance $r_n$ from the particle, and has shell thickness $\Delta r$.

The subtlety of the microscopic changes can be seen very clearly in Figure 5, which shows the rdf for the silicon-silicon, silicon-oxygen, and oxygen-oxygen pairs. Each plot includes the rdf structure for three glass quench cooling rates. The fastest quench rate studied in this work, $7.7 \times 10^{13}$ K/s, is shown in black. The slowest quench rate we were able to achieve, $5 \times 10^9$ K/s, is shown in green. An intermediate rate is shown in red, to illustrate the evolution. We see that the glass quench cooling rate does not dramatically alter the rdf. The location of the first four neighbor peaks are not significantly shifted, however the peak height and trough depth are notably sharpened for the first two nearest neighbors, indicating an increase in the short-range order. This is likely due to better relaxed states in the relative orientation of adjacent SiO$_4$ tetrahedra. This increased order, however, does not extend beyond 0.8 nm.
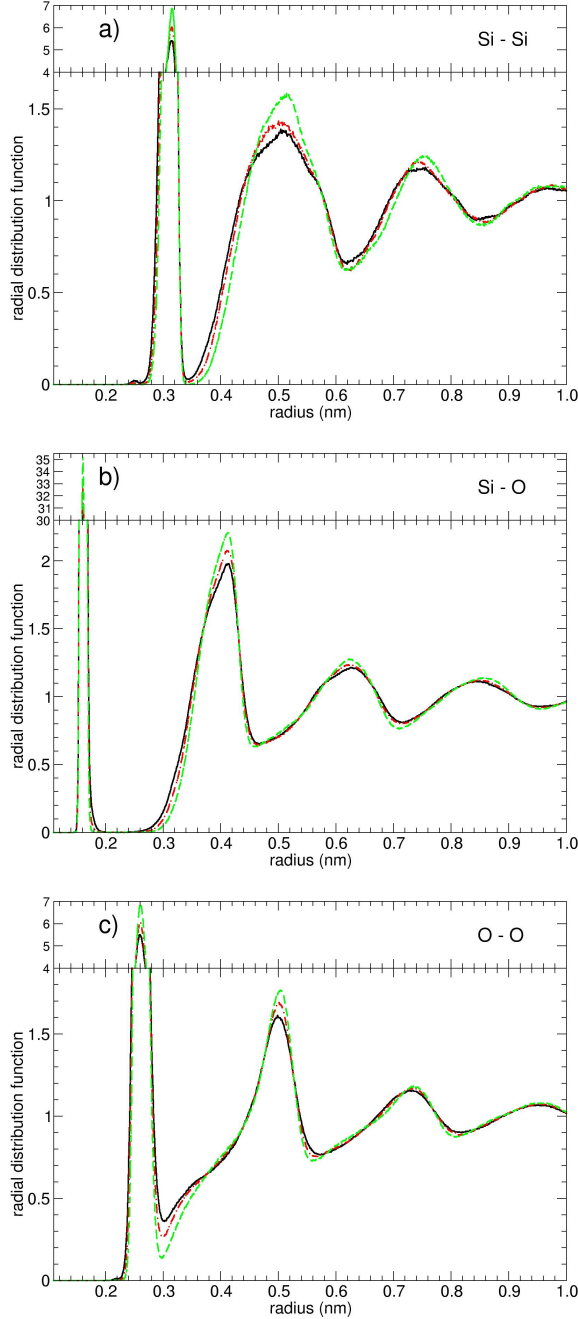
FIG. 5: (Color online) Radial distribution function plots for (a) Si - Si, (b) Si - O, and (c) O - O at 300 K after a quench ramp down from 8000 K. Three rates are shown fastest $7.7 \times 10^{13}$ in solid black, medial $3.1 \times 10^{12}$ in dash-dot red and slowest $5 \times 10^{9}$ in dash green.
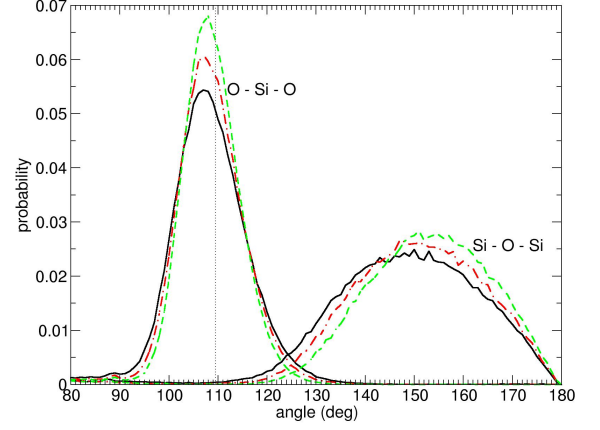


FIG. 6: (Color online) Distribution functions for the Si-O-Si and O-Si-O angles plotted together. Three rates are shown, fastest $7.7 \times 10^{13}$ in solid black, medial $3.1 \times 10^{12}$ in dash-dot red and slowest $5 \times 10^{9}$ dash green. The vertical line is the ideal tetrahedral angle.

In Figure 6 we show the angular distribution probabilities for the O-Si-O and Si-O-Si angles in the $SiO_2$ structure for three cooling rates.. The O-Si-O angle is a measure of the distortion of the tetrahedral building block structure. The Si-O-Si angle measures the arrangement of these tetrahedra elements relative to each other. The O-Si-O, as expected, is peaked near the tetrahedral angle, agreeing well with experimental measures. We see that with decreasing cooling rate, the angle distribution becomes more sharply peaked and the peak shifts very slightly toward the ideal angle. The Si-O-Si angle peak, on the other hand, does not sharpen with slower cooling rates, but does shift to larger angle by approximately 5 degrees. Very similar observations were made by Vollmayr, *et al.* in a faster range of cooling rates. We note, as they do, that the trends in Si-O-Si angle indicate a more open structure with decreased cooling rate, which is consistent with observed lower density final glasses.

These measures of glass properties as a function of cooling rate indicate that BKS glasses depend significantly on the cooling rates used to create them. Extrapolation of these properties across many orders of magnitude is challenging, as demonstrated by these studies, which indicate anticipated trends in properties can't always be reliably extrapolated from faster cooling rate data. This is seen to be the case specifically in both macroscopic properties such as thermal expansion and microscopic properties such as coordination number. In terms of agreement with experimental measures, it may be that further decrease in cooling rate does not improve the BKS glass properties. While the density would likely improve, the thermal expansion which is already below measured values, is likely to continue to drop. If this is the case, then a cooling rate of $5 \times 10^{10}$ K/s may be the optimal rate of cooling for agreement with experimentally measured properties.

### B. Viscoelastic stress relaxation in silica

We study the viscoelastic behavior of silica glasses and melts across nine decades of time by taking femtosecond time resolution simulations out to microsecond sim-

ulation durations. Two defining viscoelastic behaviors - versus elastic media - are the relaxation of stress over time, and the temperature dependence of this relaxation [28]. Viscoelastic materials alleviate internal stresses by internal structural changes, but this response takes a characteristic time which is a function of temperature. This property is well-studied in polymeric systems [29–31], where the timescales for relaxation can be on the order of minutes to hours. The phenomenon has also been studied in glass systems experimentally [32, 33].

We studied stress relaxation by instantaneously compressing an equilibrated glass isotropically and measuring the total virial pressure on the system as a function of time while holding the compressed volume constant. We defined the bulk stress relaxation modulus, K, as

$$K(t) = -V \frac{\Delta P(t)}{\Delta V} \qquad (5)$$

where $V$ is the volume of the glass sample, $\Delta V$ is the amount of initial volume reduction, and P is the total system pressure. K is a function of time through the pressure, which can change with time due to structural relaxation within the glass. This relaxation is a signature of viscoelastic response, versus the typical elastic response in solids. We conducted a series of simulations, with 3% initial strain, at several temperatures varying from 3500 K to 1000 K. These temperates span the previously calculated glass transition temperature. The principle of time-temperature superposition [34] predicts that the relaxation of the modulus, $K$ will depend on the temperature, and that the relaxation dynamics at each temperature will follow the same master curve in stress vs. log(time), which is only shifted horizontally in log(time) to account for response rates at different temperatures.

Figure 7a shows the time evolution of $K$ for six different temperatures, running from 3500 K down to 1000 K in 500 K increments. The curves for each temperature exhibit an initial plateau modulus, $K_0$, of approximately 50 GPa followed by a drop in the modulus to a final plateau value, $K_f$, of approximately 15 GPa. For the higher temperatures the initial plateau is extremely brief or not seen, while for the lowest temperatures the transition and final plateau are not observed even in the timeframe of these extremely long simulations. Although direct comparison is not possible, the experimentally measured bulk modulus of 36.9 GPa for fused silica at room temperature is between our values of $K_0$ and $K_f$. This value is consistent with a partial relaxation, although our partial relaxations at 1500 K only relax to approximately 43 GPa over microsecond times.

As expected, the rate of stress modulus relaxation to $K_0$ depends on the temperature of the sample. The fastest relaxation occurs at 3500 K, where the system relaxation is complete within 100 ps. At 3000 K, this same process takes approximately 10 times longer. At 2500 K and 2000 K, only very slight stress relaxation has occurred in the first nanosecond, a typical simulation duration for molecular dynamics system equilibra-
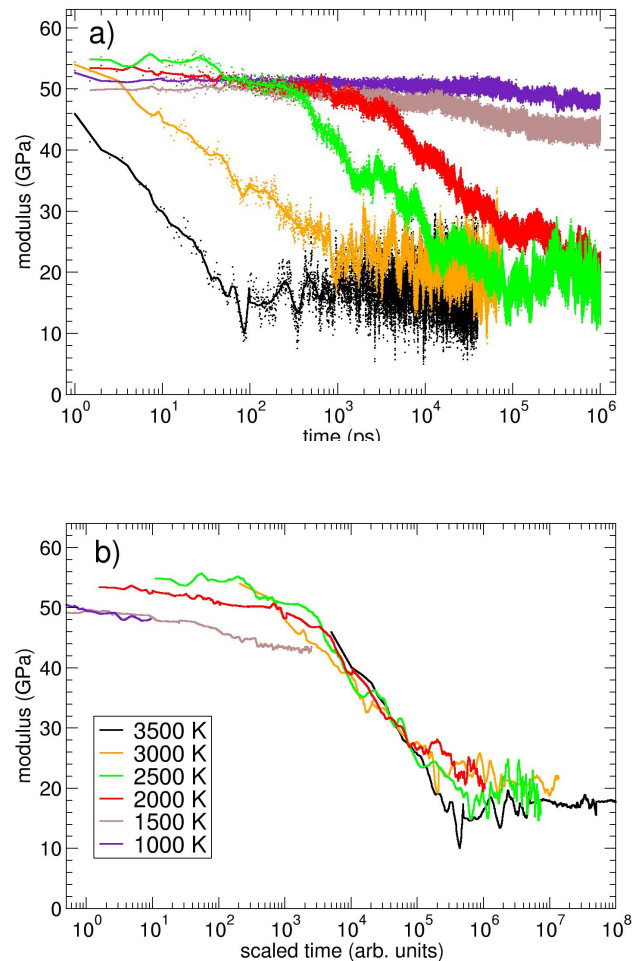


FIG. 7: (Color online) (a) The bulk stress relaxation modulus plotted vs log time plotted from picosecond to microsecond times for temperatures from 3500 to 1000 K. (b) The same data, smoothed and shifted horizontally, collapse to show the master curve for silica.

tion, however, these systems ultimately reach $K_0$, but only after 100 and 1000 ns, respectively. It should be stressed, that these are extremely long simulations – far longer than what would ordinarily be used to equilibrate a glass system. On timescales typical to molecular dynamics ( < 1 ns), these viscoelastic glasses would appear elastic.

The Figure 7b shows the same relaxation data, but each relaxation curve is smoothed and displaced horizontally by a shift factor, $a_T(T)$. The horizontal shift, $a_T(T)$, is determined for each temperature's curve by scaling time until all curves appear to best collapse. If a feature of the master relaxation curve occurs at $t_o$ before and at $t_{\text{scaled}}$ is scaled time after the shift, then $a_T = t_o/t_{\text{scaled}}$. Here we have arbitrarily selected $a_T(T = 2000K) = 1$. The data forms a reasonable
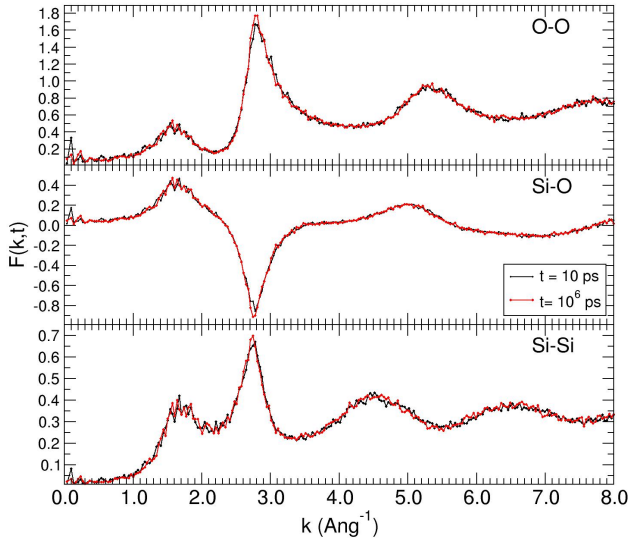
FIG. 8: (Color online) Partial intermediate scattering function before and after stress relaxation at 2000 K.

master curve for BKS silica which spans nine decades of time. No vertical shift was necessary to achieve this collapse of data. The two lowest temperature simulations, 1000 and 1500 K, exhibited only slight relaxation over the timescales of microseconds. Therefore, it was difficult to determine the appropriate horizontal shift factor, $a_T$ for these curves. In these cases, the data was shifted by the minimum factor which was consistent with the master curve.

Figure 8 shows the structure of the glass before and after stress relaxation for the 2000 K stress relaxation
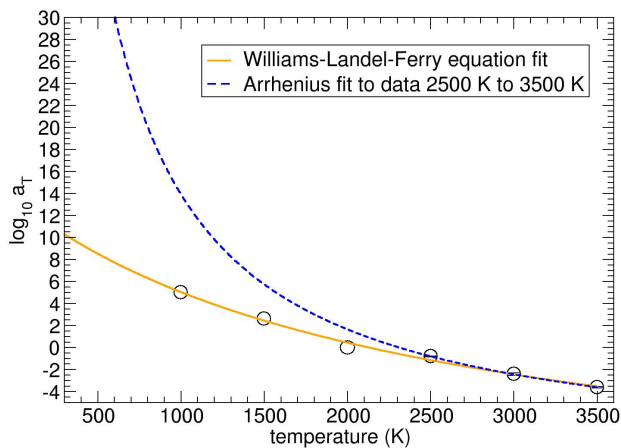


FIG. 9: (Color online) The log of the shift factor plotted vs the temperature. The data are fit two both Arrhenius and WLF theories. Error bars are smaller than the data points in the plot.

through the partial intermediate scattering function.

$$F_{ab}(k,t) = \frac{1}{N} \sum_{i=1}^{N_a} \sum_{j=1}^{N_b} e^{i\mathbf{k}\cdot(\mathbf{r}_i(t)-\mathbf{r}_j(t))} \quad (6)$$

where $N$ is the number of atoms, $\mathbf{k}$ is the reciprocal space vector, $\mathbf{r}$ is the real space position and $a$ and $b$ refer to the atom type. The response shown here, for 2000 K, is indicative of similar plots for all temperatures measured. We see that the significant stress relaxation is the result of only very subtle structural change within the glass. In fact, with the exception of small differences in the peak at the $k = 1.75$ Å$^{-1}$ we see that the before and after scattering functions appear identical within the fluctuations. A more thorough study of the correlation between structural and stress relaxation on these timescales could be very interesting.

Two theories predict the shift values, $a_T$, near the glass transition, the Williams-Landel-Ferry (WLF) theory [35] and below $T_g$, the Arrhenius behavior. WLF theory gives for the shift factor,

$$\log_{10} a_T = \frac{-C_1 \times (T - T_0)}{C_2 + T - T_0} \quad (7)$$

while the Arrhenius behavior is given by,

$$\log_{10} a_T = A(\frac{1}{T} - \frac{1}{T_0}) \quad (8)$$

where $C_1$, $C_2$ and $A$ are fit parameters and $T_0$ is usually associated with $T_g$ for the material.

Figure 9 shows the calculated shift factors extracted from Figure 7b versus temperature. These data were fit to WLF theory with with Eq. 7 with parameters, $C_1 = 15.11$, $C_2 = 4511$ and $T_0 = 2128$ K. We also fit to Arrhenius theory with Eq.8 to data in the temperature range where silica has previously been shown to exhibit Arrhenius behavior (i.e. below 3500 K [15] and above $T_g$ [18, 28]. The Arrhenius fit yeilded fit paraemters of $A = 24550$ and $T_0 = 2311$ K. As discussed above, the shift factors at 1000 and 1500 K are only lower bounds because these systems did not fully relax to $K_0$ on simulation timescales. These predicted shifts in the relaxation times can be used to predict the degree of relaxation which would occur in simulations too long to conduct. Below $T_g$, WLF theory is generally a better estimate for the shift factors associated with stress relaxation [28]. We believe these fits could be used to determine parameters for accelerated dynamics simulations in which extremely long relaxation times are artificially modeled through manipulation of an effective temperature.

## IV.   CONCLUSIONS

In conclusion, we have studied statics and dynamics of a simple, but accurate, glass model out to microsecond times. These simulation times, represented a two to

three order of magnitude improvement over previously published studies of glass cooling rate effects, and provided 9 decades of temporal evolution for the study of viscoelastic properties near the glass transition temperature.

We found that glasses formed by cooling rates from $7.7 \times 10^{13}$ K/s to $5 \times 10^9$ K/s showed significant differences in their final static properties. Over this range of cooling rates, the final glass density dropped by 4.5 %, from 2.31 g/cc to 2.22 g/cc. The thermal expansion coefficient of the final glass dropped from $3.15 \times 10^{-6}$ 1/K to $0.25 \times 10^{-6}$ 1/K, and notably fell below the experimental value. Both of these macroscopic observables deviated from linear trends in $\log(\gamma)$ extrapolated from faster cooling rates. The microscopic structure was measured in the coordination number, the radial distribution functions and angular probabilities of the glasses. The observed macroscopic changes were achieved with relatively modest changes to glass structure. A drop in the over-coordination of silicon and oxygen, and increasing Si-O-Si angle particularly point to an opening of the glass structure that is consistent with decreasing density. In the rdf, slightly deeper wells and sharper peaks of the second and third neighbor peaks were observed, with little change in the first peak, and no significant shift in peak locations.

We were able to clearly observe viscoelastic behavior in the long time behavior of silica melts and glasses. Time-temperature superposition was observed in the stress relaxation bulk modulus extracted from six temperatures, ranging from 3500 K to 1000 K. The master curve for stress modulus relaxation was extracted and shift factors were compared with theory. This demonstration of robust time-temperature superposition in silica simulation will lead to well-characterized accelerated stress relaxation techniques.

[1] A. Pedone, J. Phys. Chem. C **113**, 20773 (2009).
[2] K. Binder, J. Non-cryst. Solids **274**, 332 (2000).
[3] J. Du and A. Cormack, J. Non-cryst. Solids **349**, 66 (2004).
[4] K. Vollmayr-Lee, R. Bjorkquist, and L. M. Chambers, Phys. Rev. Lett. **110**, 017801 (2013).
[5] K. Vollmayr-Lee, J. Roman, and J. Horbach, Phys. Rev. E **81**, 061203 (2010).
[6] A. Kerrache, V. Teboul, D. Guichaoua, and A. Monteil, J. Non-cryst. Solids **322**, 41 (2003).
[7] B. Mantisi, A. Tanguy, G. Kermouche, and E. Barthel, Eur. Phys. J. B **85**, 1 (2012).
[8] Y. Liang, C. R. Miranda, and S. Scandolo, High Pressure Research **28**, 35 (2008).
[9] F. Yuan and L. Huang, J. Non-cryst. Solids **358**, 3481 (2012).
[10] J. Ashwin, E. Bouchbinder, and I. Procaccia, Phys. Rev. E **87**, 042310 (2013).
[11] B. M. Lee, H. K. Baik, B. S. Seong, S. Munetoh, and T. Motooka, Comp. Mater. Sci. **37**, 203 (2006).
[12] A. Tilocca, J. Chem. Phys. **139**, 114501 (2013).
[13] V. V. Hoang and T. Odagaki, Philos. Mag. **88**, 1461 (2008).
[14] B. Van Beest, G. J. Kramer, and R. Van Santen, Phys. Rev. Lett. **64**, 1955 (1990).
[15] J. Horbach and W. Kob, Phys. Rev. B **60**, 3169 (1999).
[16] D. Price and J. Carpenter, J. Non-cryst. Solids **92**, 153 (1987).
[17] K.-U. Hess, D. Dingwell, and E. Rössler, Chem. Geol. **128**, 155 (1996).
[18] K. Vollmayr, W. Kob, and K. Binder, Phys. Rev. B **54**, 15808 (1996).
[19] R. Brückner, J. Non-cryst. Solids **5**, 123 (1970).
[20] J. E. Shelby, J. Non-cryst. Solids **349**, 331 (2004).
[21] C. Angell, J. Phys. Chem. Solids **49**, 863 (1988).
[22] C. Angell, J. Non-Cryst. Solids **131-133**, 13 (1991).
[23] I. Saika-Voivod, P. H. Poole, and F. Sciortino, Nature **412**, 514 (2001).
[24] S. J. Plimpton, J. Comp. Phys. **117**, 1 (1995), LAMMPS code http://lammps.sandia.gov.
[25] R. Hockney and J. Eastwood, Hilger, Bristol (1988).
[26] O. Mazurin, M. Streltsina, and T. Shvaiko-Shvaikovskaya, Elsevier Science Publishers (1983).
[27] D. C. Rapaport, *The art of molecular dynamics simulation* (Cambridge University Press, Cambridge, 1995).
[28] J. Dealy, and D. Plazek, Theol. Bull. **78**, 16 (2009).
[29] A. V. Tobolsky, J. Appl. Phys. **27**, 673 (1956).
[30] J. Baschnagel, K. Binder, and H.-P. Wittmann, J. Phys. Cond. Matter **5**, 1597 (1993).
[31] C. Bennemann, J. Baschnagel, W. Paul, and K. Binder, Comput. Theor. Polymer Sci. **9**, 217 (1999).
[32] D. Larsen, J. Mills, and J. Sievert, J. Non-Cryst. Solids **14**, 269 (1974).
[33] G. Bartenev and N. Scheglova, J. Non-Cryst. Solids **37**, 285 (1980).
[34] R. Christensen, *Theory of viscoelasticity: an introduction* (Elsevier, 1982).
[35] M. L. Williams, R. F. Landel, and J. D. Ferry, J. Amer. Chem. Soc. **77**, 3701 (1955).